Straightforward Design Strategy toward 3D Near-Net-Shape Stoichiometric SiC Parts

Maxime Cheype, Vincent Pateloup, Samuel Bernard

Straightforward design strategy towards 3D near-net-shape stoichiometric SiC parts

Maxime Cheype, Vincent Pateloup, Samuel Bernard**

[*] Dr. Maxime Cheype

IRCER, CNRS, Univ. Limoges, Limoges, France

E-mail: maxime.cheype@unilim.fr

Dr. Vincent Pateloup

IRCER, CNRS, Univ. Limoges, Limoges, France

[*] Dr. Samuel Bernard

IRCER, CNRS, Univ. Limoges, Limoges, France

E-mail: samuel.bernard@unilim.fr

Keywords: Silicon carbide, carbon-rich polycarbosilane, FDM

Fused deposition modeling (FDM), traditionally reserved for thermoplastics, is modified here with a granule-based extrusion head to be extended to advanced nonoxide ceramics via a straightforward design strategy that considers the shaping opportunities and the chemical richness offered by preceramic polymers. Specifically, 3D near-net-shape stoichiometric silicon carbide (SiC) objects are designed by manipulating the key features of a commercially available polycarbosilane (fusibility, high carbon content, relatively high SiC yield). In the early stage of the process, the carbon-rich polycarbosilane is first mixed with Si and SiC fillers and then thermolyzed at 120 °C to increase polymer branching while offering tailored rheological properties during the subsequent extrusion process at 90 ÆC and adequate shape retention once extruded. This allows for the design of tailored and complex 3D complex polycarbosilane-based architectures with features down to 400 µm. Polymer-based parts are further converted into 3D stoichiometric SiC objects with quasi-near-net-shape—a volume shrinkage reduced to 9.1% is measured—by heat treatment at a temperature as low as 1400 ÆC (argon flow). Given the flexibility to tune the preceramic polymer chemical and rheological properties, a new combined design approach is leveraged to generate bespoke advanced ceramics with a high freedom in geometry complexity.

1. Introduction

Materials discovery is a key element to meet the technological challenges of the coming decades in the innovation cycle of energy and aerospace technologies. In such technologies, silicon carbide (SiC) – discovered more than 130 years ago - is identified as a major material. SiC offers unique features like light weight, excellent thermal shock resistance performance, high strength and a high temperature oxidation resistance. These valuable properties make SiC an ideal choice for various high temperature applications in high tech domains as telescope mirrors[1,2], as solar absorbers for concentrated solar power (CSP)[3,4] or as heat

exchangers[5–7]. However, manufacturing complex-shaped SiC parts – which requires very high temperature and/or pressure to obtain a dense material due to its strong covalent bonding[8,9] - faces extremely difficult challenges in terms of shape complexity.

As an innovative technology, additive manufacturing (AM) represents a technology that can disrupt the global supply chain and eliminate resource waste and bottlenecks.[10] It has recently renewed the vision of designing objects by giving access to new and complex architectures and topologies of materials such as plastics, metals or ceramics which cannot be achievable by more conventional manufacturing technologies.[11]

AM of SiC is a hot topic[12–14]: because SiC cannot be cast or machined easily, AM would enable a big leap in geometrical flexibility by considering that SiC is best suited for complex and advanced parts. Thus, different strategies can be envisionned such as stereolithography[15-16], Direct ink writing (DIW)[17-18], Gel casting using 3D-printed polymer skeleton[19], selective laser sintering (SLS)[20], binder jet printing[21] and extrusion-based AM technologies[22-23]. They are mainly derived from powders.[24] Among them, the extrusion process looks as the most promising way to design complex shapes of advanced ceramics as large components with flexibility, reduced manufacturing lead times, high precision and low cost.[25] However, a major drawback is the incredible difficulty to overcome the debinding and densification stages[13,22]: very high temperatures (can be more than 2000 °C) and high pressure, dimensional restrictions, significant presence of residual silicon (Si) and/or carbon (C), presence of sintering additives as impurities and/or presence of amorphous phases.

Reaction bonding by molten silicon infiltration[26-28] – achieved by a capillary force between silicon and a carbon-based porous preform - remains the most effective densification process according to the short processing time and the relatively low temperature (above the melting point of silicon, 1410 °C)[29] compared with traditional sintering methods. However, major issues such as the high parametric sensitivity, the exothermicity of the reaction between molten silicon and carbon and the permeability reduction implied by SiC formation complicate the infiltration and conversion process.[30] If not precisely controlled, the residual carbon - due to sluggish reactivity of the larger carbon particles - and the residual silicon - due to the lack of carbon required for reaction with silicon or the formation of cracks in the carbon preform - will significantly reduce the application of these materials at high temperature, both under inert (melting of Si) and oxidative (formation of SiO/SiO_2 and CO/CO_2) atmospheres.

Hence, despite continuing advances, there are no current examples that fully exploit the potential of extrusion-based AM to create complex stoichiometric SiC parts in a simple process at a relatively low temperature (below 1800 °C) without non desired elements.

We propose to diverge from traditional fabrication methods of 3D SiC parts and move toward a combined approach - Fused Deposition Modeling (FDM), a processing technique that, up to this point, has been mainly reserved for thermoplastics coupled with the Polymer-Derived Ceramics (PDC) route as a ceramic synthesis route - that has never been deployed to design 3D stoechiometric SiC.

FDM, also known as fused filament fabrication (FFF)[31], is an AM process which builds parts layer by layer by selectively depositing a melted material in a predetermined path. It uses thermoplastics that come in filaments to form the final physical objects. FDM has achieved high rates of production at full industrial scale, and innovation in this process has the opportunity for significant global benefits.

The PDC route[32-33] uses preceramic polymers as precursors of the targeted ceramics which offers shaping capabilities – using forming techniques usually applied for thermoplastic polymers such as AM[34-36] - in a way not known for alternative ceramic design approaches. Indeed, the viscosity and elastic properties of preceramic polymers can be tuned and converted to filaments via melt-extrusion.[37-40] Therefore, they seem to be promising for the printing of 3D objects using FDM. However, all FDM-PDC reports mix preceramic polymers with thermoplastic binder components (*e.g.*, polypropylene) as suitable additives to obtain appropriate and stable composite filaments as well as defect-free structures.[41-43] Thus, high volume shrinkage occurs and for SiC, significant presence of free carbon is observed.[43]

Herein, we take advantage of the shaping richness and chemical flexibility of preceramic polymers as single-source precursors (*i.e.*, without thermoplastic binder components) to implement an extrusion AM technology derived from FDM as a new landscape in the field of SiC. The design process is straightforward (**Figure 1a**) and makes use of i) mixing in a controlled mass ratio a thermoplastic carbon-rich polycarbosilane (PCS) used as a binder containing Si and SiC particles to form after thermolysis at 120 °C a tailor-made ink, ii) extruding the as-prepared ink as a melt to deliver – via a granule-based FDM process - on-demand 3D parts and iii) heat-treatment to form 3D near-net-shape stoichiometric SiC parts with high resolution. The potential impact of this work is demonstrated in the applications for i) lightweight opto-mechanical systems in which we designed mirrors (**Figure 1a**), ii) CSP in which we designed high-flux concentrated solar receivers (**Figure 1b**) and iii) thermal management in which we designed heat exchangers (**Figure 1c**); all architectures must work in adverse environments (high temperature) **(Figure 1d**). Below are our major highlights.

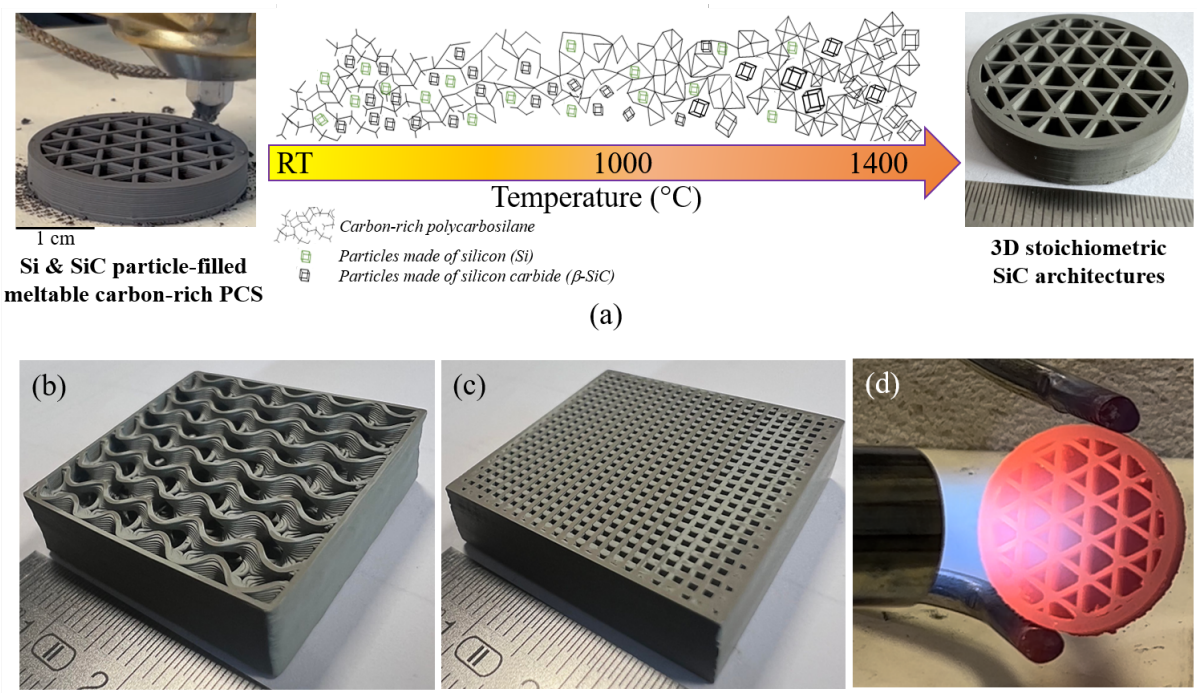

Figure 1. Flow diagram of the manufacturing process (a) and examples of complex shapes that can be prepared (a-c) for high temperature applications (d).

2. Results and Discussion

Central to our process offering unparallel flexibility is the commercially available polymer StarPCS™ SMP-730[44] we labelled **SMP-730**. This non conventional PCS (because of its high carbon content, *see later*) is engineered to process like a thermoplastic polymer and is capable of being repeatedly melted and solidified (*See Figure 1SIa in ESI*) at low temperature, below its decomposition. Furthermore, it can be converted into ceramics with a relatively high ceramic yield (65-67 $_{wt}$%). However, **SMP-730** brings two major drawbacks to form 3D SiC:

1) Its viscosity as a melt (around 5 Pa.s at 127 °C (*See Figure 1SIb in ESI*)) and its glass transition temperature (T_g = +10 °C) are both too low to allow for a stable extrusion – it wets and spreads upon exiting the nozzle - and to keep the cohesion of the shape after extrusion – it lacks the ability to support itself.
2) It displays an empirical formula of $Si_{1.0}C_{4.1}H_{7.0}N_{0.1}O_{0.2}$ (**Table 1**) leading to a calculated atomic C:Si ratio of 4.1 which is very far from the stoichiometry (C:Si = 1.0). Hence and besides the presence of oxygen, **SMP-730** behaves like a C-rich PCS which inherently generates, after heat-treatment at a minimum temperature of 1400 °C, SiC with a relatively high free C content ($Si_{1.0}C_{2.80}O_{0.4}$ for **SMP-730_14** (**Table 1** given a calculated carbon phase content of around 32.9 $_{wt}$%) that could trigger

undesired reactions at high temperature and affect some of the properties (stability in harsh environment) of the materials.

Table 1. Elemental analysis of the **SMP-730** (& **R120**), **SMP-730_14** (& **R120_14**), **SMP-730_18** (& **R120_18**), **$Si_{12.6}$@R120_14** and **$Si_{12.6}$@R120_18** samples and their corresponding empirical formula.

Samples	O (wt%)	N (wt%)	H (wt%)	C (wt%)	Si (wt%)	Empirical formula[a)]
SMP-730 & R120	4.0	1.0	7.7	55.2	32.1	$Si_{1.0}C_{4.1}H_{7.0}N_{0.1}O_{0.2}$
SMP-730 & R120_14	6.9	0.0	0.1	50.3	42.7	$Si_{1.0}C_{2.8}O_{0.4}$
SMP-730 & R120_18	0.3	0.1	0.0	53.1	46.5	$Si_{1.0}C_{2.7}$
$Si_{12.6}$@R120_14	5.2	0.0	0.0	28.9	67.9	$Si_{1.0}C_{1.0}O_{0.1}$
$Si_{12.6}$@R120_18	0.2	0.1	0.0	31.1	68.6	$Si_{1.0}C_{1.0}$

[a)]Referenced for $Si_{1.0}$

We turn these drawbacks into advantages to formulate a tailor-made ink, composed of **SMP-730** as the preceramic polymer, Si powders as active fillers and SiC powders as passive fillers; a mixture which is thermolyzed at 120 °C prior micro-extrusion.

The thermolysis at 120 °C only affects the **SMP-730** compound: it delivers a hard/glassy compound labelled **R120** with a glass transition temperature (T_g) increased by more than 50 % (T_g = +16.3 °C) compared with the T_g of pristine **SMP-730** (T_g = +10.0 °C). However, the viscosity of the **R120** sample as a melt was still too low for a stable extrusion, *i.e.*, similar to the pristine polymer (*See Figure 1SIb in ESI*). Hence, a controlled content of Si and SiC powders has been further added to modify the rheology that imparts both shear thinning behaviour and shear yield stress of **R120**. In addition, this strategy will allow reducing the volume shrinkage of the 3D printed part upon heat-treatment of **R120** to ultimately form stoechiometric SiC.

We hypothesized that Si powders would react at high temperature with free carbon - *in situ* formed in the material upon heat-treatment of **SMP-730** (and **R120**) - to deliver a purely SiC phase based on the Active Filler-controlled Pyrolysis (AFCOP) concept published by P. Greil *et al.*.[45] Thus, based on the excess of carbon in the **SMP-730_14** sample (**Table 1**), we adjusted the quantity of Si powders to be introduced in **SMP-730** (in solution in toluene) at

12.6 $_{vol}$% (**Si$_{12.6}$@SMP-730**) before achieving solvent extraction (*See Experimental Section*) and then a heat-treatment at 120 °C to deliver the **Si$_{12.6}$@R120** sample as described above. **Si$_{12.6}$@R120** could deliver a material with the targeted Si:C ratio of 1 after heat-treatment at 1400 °C under argon as highlighted by elemental analysis (**Table 1**) with the sample labelled **Si$_{12.6}$@R120_14**. This ratio is confirmed in the sample obtained at 1800 °C (**Si$_{12.6}$@R120_18**, **Table 1**).

To allow the **Si$_{12.6}$@R120** sample for a stable extrusion as a melt – a viscosity of 200 Pa.s at 110-115 °C (*See Figure 1SIb in ESI*) has been measured which is still too low for the process – we added SiC powders (which are inert with their close environment (*i.e.*, polymer)) to this formulation (before the thermolysis at 120 °C) to generate a Si and SiC powder-filled **SMP-730** sample. It has been found that 40 $_{vol}$% of SiC powders mixed in solution with the **Si$_{12.6}$@SMP-730** sample before solvent removal (*See Experimental Section*) could deliver after heat-treated at 120 °C a tailor-made ink labelled **Si$_{12.6}$SiC$_{40.0}$@R120**. This ink reported an evolution profile of the viscosity similar to those of **SMP-730**, **R120** and **Si$_{12.6}$@R120** - although much more jerky - with a strong increment along the Y-axis : a melt-viscosity above 2×10^4 Pa.s is measured, thereby 100 orders of magnitude higher than that of **Si$_{12.6}$@R120** (*See Figure 1SIb in ESI*). Thus, the **Si$_{12.6}$SiC$_{40.0}$@R120** sample could readily flow at 90 °C – without blocking extrusion - and embodies the essential rheological properties required for the granule-based FDM process. The rheological behaviour of **Si$_{12.6}$SiC$_{40.0}$@R120** at its extrusion temperature (90 °C) is shown in **Figures 2**.

The complex viscosity η* of the **Si$_{12.6}$SiC$_{40.0}$@R120** sample continuously and strongly decreases in the oscillatory frequency range 0.10-100 s^{-1}, indicating clearly its strong shear-thinning behaviour. Such a behaviour is expected to allow the ink to flow through micro-nozzles, due to the viscosity decrease of several orders of magnitude as a result of an increase of oscillatory frequency - or shear rate which is calculated from the oscillatory frequency and geometry strain constant - upon the application of an external force on the ink. Regarding storage and loss moduli as a function of test frequency, it can be seen that the **Si$_{12.6}$SiC$_{40.0}$@R120** sample reveals an increase of the magnitude of G'' with increasing oscillatory frequency from 1 s^{-1} which is due to the higher energy required for molecular viscous response.[46] The slighter increase of the magnitude of G' for melts is attributed to a decrease in time available for molecular relaxation.[46] The elastic behaviour of the **Si$_{12.6}$SiC$_{40.0}$@R120** sample remains predominant (*i.e.*, G' is larger than G'') up to an oscillatory frequency of 20 s^{-1} at which a crossover point between the two moduli curves occurs. It corresponds to a shear rate of 133 s^{-1}. Thus, the viscous component (G'') becomes

predominant – tanδ > 1 - at high oscillatory frequency (thereby, at a high shear rate) indicating that the material has a predominant liquid-like behaviour as a prerequisite to allow it flowing inside the nozzle.

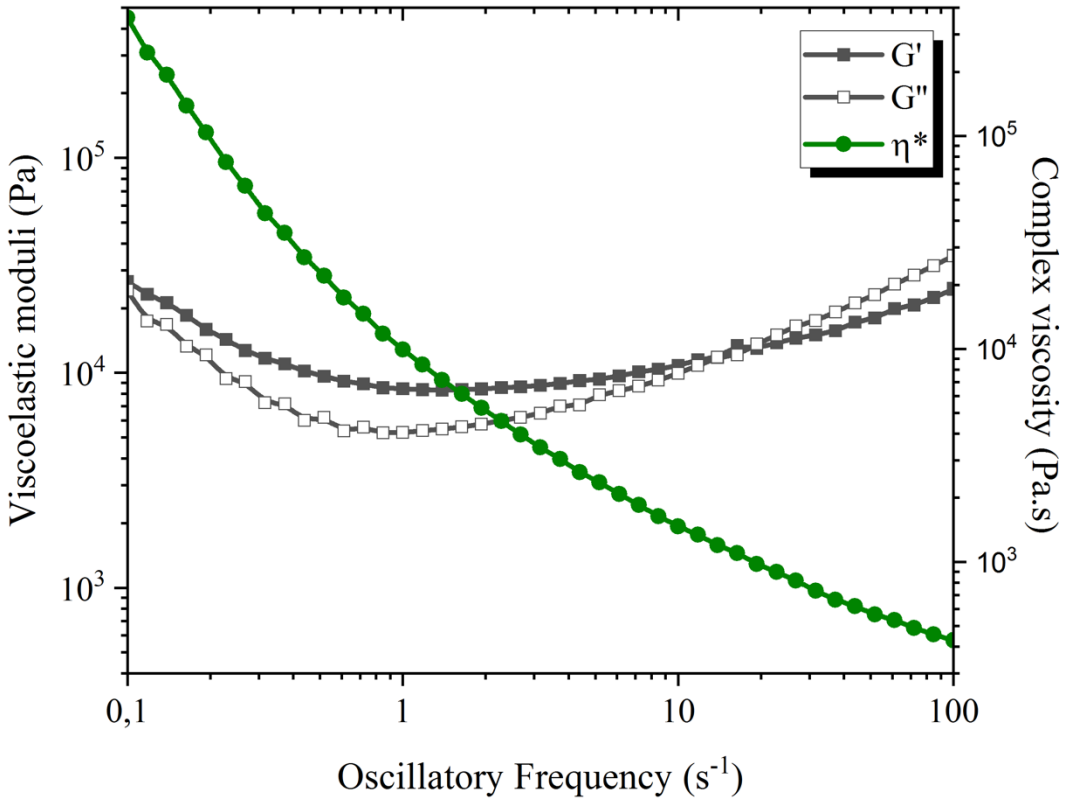

Figure 2. Log-log plots of complex viscosity and storage and loss moduli as a function of oscillatory frequency for the **$Si_{12.6}SiC_{40.0}$@R120** sample at 90 °C.

Hence, extrusion of the **$Si_{12.6}SiC_{40.0}$@R120** sample is expected to occur at relatively high extrusion velocity. Then, the **$Si_{12.6}SiC_{40.0}$@R120** sample develops sufficiently high shear elastic modulus (*G′* larger than *G″*) after exiting the micronozzle (because of the decrease of the shear rate) to maintain its printed filamentary shape during the cooling phase below the nozzle and to provide adequate shape retention. The as-printed filamentary shape follows the architecture imposed by the CAO program in a stable process to form 3D parts that maintain the shape and do not collapse under the weight of multilayers deposited on them as shown on the video capture of the extrusion proces (**Figure 1a,** left).

As-designed 3D raw parts could be next transformed into quasi near net shape 3D SiC architectures - a volume shrinkage as low as 9.1 % was measured – by a further heat-treatment at 1400 °C in flowing argon (**Figure 1**). The decomposition of the polymer content

of the ink, *i.e.*, **R120**, occurred in a first step in the temperature range 120 – 750 °C (*See Figure 2SI in ESI*) before a plateau to deliver the samples labelled **$Si_{12.6}SiC_{40.0}$@R120_14** with a weight loss as low as 10 % to be compared to 32.5 % for the **R120** sample. We can particularly highlight the high resolution of the structure which has been designed by the granule-based FDM process (**Figure 3a**).

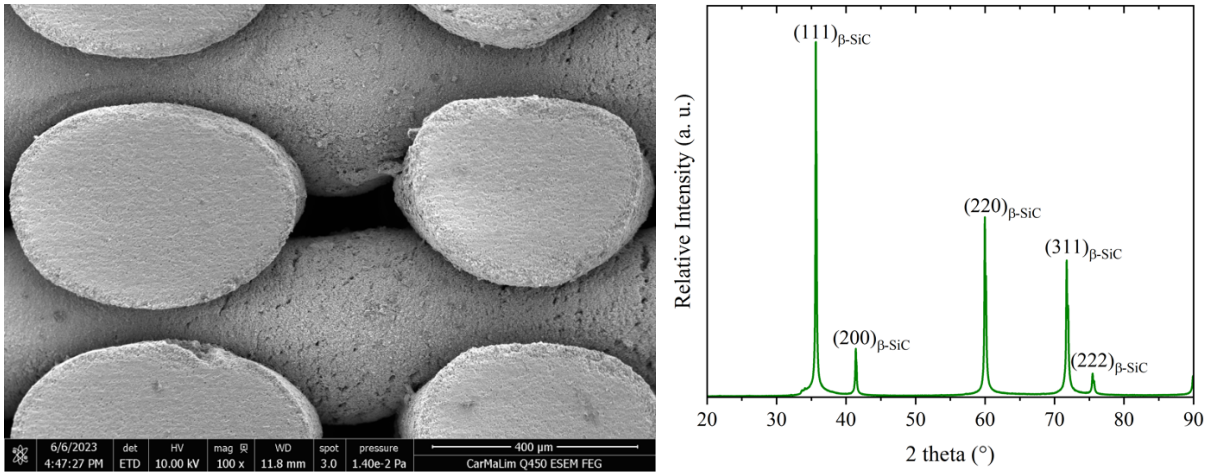

(a) (b)

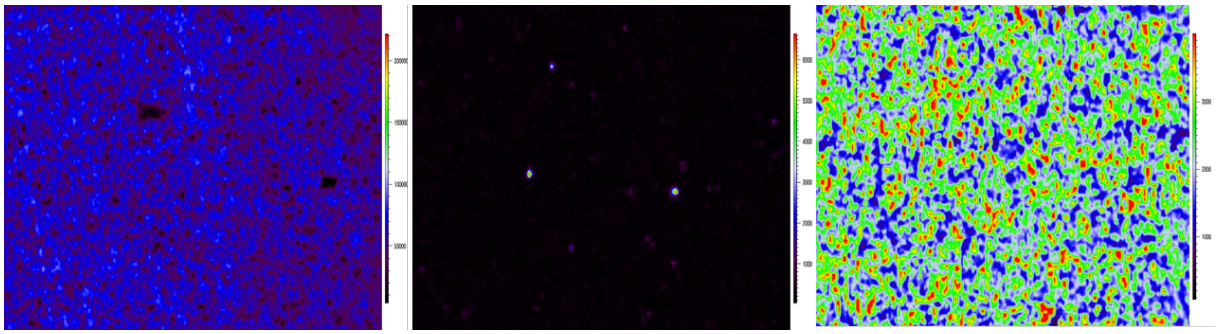

(c)

Figure 3. Cross-sectional SEM image of the lattice structure of the 3D-printed **$Si_{12.6}SiC_{40.0}$@R120_14** sample which reveals that the filamentary shape is retained after heat-treatment to 1400°C (a), XRD pattern of the 3D-printed **$Si_{12.6}SiC_{40.0}$@R120_14** sample (b) and 200 × 200 µm^2 Raman maps of the 3D-printed **$Si_{12.6}SiC_{40.0}$@R120_14** sample collected with a step size of 1.3 µm : C (left), Si (middle), SiC (right) (c).

Although Archimedes' measurements showed a relative density of 71.0 %, the SEM observations of a typical lattice structure of the 3D-printed **$Si_{12.6}SiC_{40.0}$@R120_14** sample show a dense and uniform microstructure in the bulk with a reduced presence of porosities at the surface (**Figure 3a**). This is confirmed through the observation of SEM images at higher magnification (*See Figure 3SI in ESI*). This indicates that the reduced relative density is

probably due to the presence of internal defects and bubbles while the uniform microstructure demonstrates that the fillers are homogeneously distributed and trapped in the matrix derived from **SMP-730** (and **R120**).

The X-ray diffraction (XRD) pattern (**Figure 3b**) of the 3D-printed **$Si_{12.6}SiC_{40.0}$@R120_14** sample identifies a single crystalline phase corresponding to β-SiC (JCPDS 00-029-1129) as confirmed through the presence of peaks at 35.6° (111), 41.4° (200), 60° (220), 71.8° (311) and 75.3° (222) without traces of Si (JCPDS 04-001-7247). The presence of an additional highly diffuse peak at 33.7° can be explained by the presence of faults in the regular cubic stacking sequences.[47] Si was identified in the XRD pattern of the 3D-printed **$Si_{12.6}SiC_{40.0}$@R120_10** sample through the emergence of peaks at 28.4° (111), 47.3° (220), 56.1° (311), 69.1° (400), 76.4° (331), 88.0° (422) along with the peaks assigned to β-SiC (*See Figure 4SI in ESI*). These peaks identify the Si and SiC fillers which have been introduced in the **R120** sample in the early stage of the process. As a consequence, the reaction of Si powders (active fillers) with the *in situ* formed sp^2 C phase occurred above 1000 °C to be achieved at 1400 °C - below the melting point of Si - and delivered a stoechiometric SiC (*See Table 1*) in a β phase (**Figure 3b**). This reaction was allowed in this temperature range most probably because of the amorphous/turbostratic state of the *in situ* formed sp^2 C phase.[45,48,49] It is important to notice that the pyrolysis of **R120** at 1000 °C (**R120_10**) and 1400 °C (**R120_14**) in flowing argon offers poorly crystallized SiC as indicated through the very diffuse peaks composing the corresponding XRD patterns (*See Figure 4SI in ESI*). A temperature of 1800 °C (**R120_18**) is required to crystallize SiC derived from the **R120** sample in a β phase (*See Figure 4SI in ESI*). The XRD pattern of the 3D-printed **$Si_{12.6}SiC_{40.0}$@R120_18** sample (*See Figure 4SI in ESI*) confirmed the formation of a single β-SiC phase.

To evidence our discussion, we reconstructed Raman maps by selecting the relevant vibrational signatures of carbon (C), silicon (Si) and silicon carbide (SiC) in collected individual Raman spectra (**Figure 3c**). Three different maps of 200 × 200 μm^2 were built for each condition in order to obtain a representative information of the surface of the 3D-printed **$Si_{12.6}SiC_{40.0}$@R120_14** sample. Spectra were recorded between 480 and 1680 cm^{-1}. Then, the maps were reconstructed according to the integrated intensity of the D and G modes of C from 1150 to 1680 cm^{-1} [48], of the LO mode of Si from 480 to 550 cm^{-1} [50] and of the TO mode of SiC from 770 to 820 cm^{-1} [51]. The warmer the color is (*i.e.* red), the more intense the corresponding band is and consequently the more the phase content is. Raman spectroscopy confirms the absence of carbon and silicon in the 3D-printed **$Si_{12.6}SiC_{40.0}$@R120_14** sample (a collection of 24 000 spectra has been done); especially by considering the high raman-

sensitivity to probe sp^2 carbon and silicon signals. This is highlighted by comparing with the Raman spectrum of the 3D-printed **$Si_{12.6}SiC_{40.0}$@R120_10** sample that clearly identified carbon and silicon phases (*See Figure 5SI in ESI*).

To extend this work beyond the chemistry-process-structure relationships of 3D SiC architectures, samples have been subjected to preliminary four-point bend flexural tests (*See Experimental Section*). Since we are dealing with new compounds, the purpose of this investigation is not to provide a detailed and statistical analysis of the mechanical properties but a first look at the robustness of as-produced 3D SiC architectures due to the non-optimized manufacturing at this stage. It is important to mention that four-point bending tests have required the design of bars (*See Figure 6SI in ESI*) representing simple and thick shapes which are quite difficult to be achieved by FDM-based process. This greatly affects the measurements of mechanical properties and this can explain why such an investigation is poorly covered in the literature.

As expected, the representative flexural curves for the 3D-printed **$Si_{12.6}SiC_{40.0}$@R120_14** sample (*See Figure 7SI in ESI*) showed a general brittle behaviour typical of ceramics and by calculating the Young's modulus from the linear region of the graph, we were able to measure a Young's modulus (E) of 163.0 GPa ± 15.9 and a flexural strength (σ) of 47.2 ± 5.5 MPa. 3D SiC parts using FDM technology[52] or DIW technology[53] demonstrated flexural strengths in the range of 30-58 MPa; thus, the 3D SiC architectures developed in this study display mechanical properties that fit with this range. However, these values are much lower than those obtained by conventional processes as the 3D-printed samples usually exhibit imperfect interlayer bonding and voids (*See. Figure 8SI in ESI for the sample with the lowest flexural strength*). It is well reported that the presence of porosity of microsize highly influences the origination and growth of cracks, leading to premature failure.[54] Based on studies conducted on the influence of porosity on mechanical properties[55–57], it is clear that a greater attention to the multiple FDM parameters is important in order to reduce defects and porosity and thus increase the mechanical properties of the final 3D architectures. One way to reduce porosity and defects in FDM printing is to increase the amount of extruded material, a technique called overextrusion[58–59] although this way can cause a "flooding" of the material between rasters. This will be investigated in a more focused paper.

3. Conclusion

In summary, we have demonstrated the feasibility of printing 3D stoechiometric SiC architectures by manipulating the key features of a commercially available PCS (fusibility,

high carbon content, relatively high yield) to be tailored for FDM-based technologies traditionally reserved for thermoplastics.

Hence, we have developed inks made of SMP-730 (C-rich PCS), Si powders (active fillers) and SiC powders (passive fillers) which could be tailored by a thermolysis at 120 °C to be then extruded via a stable granule-based FDM process at 90 °C into on-demand 3D parts. The latter were converted into quasi near-net-shape 3D SiC parts at a temperature as low as 1400 °C to ensure the formation of stoichiometric SiC. Thus, our combined process showed repeatability and reliability and it constitutes a new landscape in the AM field of SiC by breaking the current limits of AM strategies leading to SiC with disruptive and practical 3D architectures. In the present work, we conducted systematic studies to characterize the evolutive material at each step of the process and to understand the limitation and opportunities of the proposed approach. The findings of our work can be summarized as follows:

- The ink displayed a shear-thinning behaviour during extrusion allowing it to flow through micro-nozzles, and a rapide increase of the viscosity after extrusion as a result of the decrease of the angular frequency allowing the filament to keep its shape and providing adequate shape retention.
- A volume shrinkage as low as 9.1 % has been measured after heat-treatment to 1400 °C in flowing argon indicating the production of quasi near-net-shape 3D parts.
- X-ray diffraction coupled with Raman spectroscopy revealed that the *in situ* formed carbon derived from the selected polymer fully reacted with Si powders to deliver SiC at a temperature as low as 1400 °C.
- A single crystalline phase corresponding to β-SiC is delivered in final 3D architectures.

The potential impact of this work is demonstrated in the applications for lightweight opto-mechanical systems in which we designed mirrors, for CSP in which we designed high-flux concentrated solar receivers and for thermal management in which we designed heat exchangers. Additionaly, this study provides a promising pathway to develop a large range of complex architectures given the broad applicability of the proposed process. By considering the various processing parameters which can be involved, there are ample opportunities to prepare tailor-made forms of SiC, to optimize the relative density of the latter (thus their mechanical properties as well) and to extend towards more complex compositions such as composites by considering specific process parameters. These opportunities are now being

addressed. It is anticipated that this will lead to host of structural and functional applications for a new generation of materials.

4. Experimental Section/Methods

Materials: The manipulation of the different compounds, *i.e.*, the polymer, the solvent and the fillers, is carried out in a purified argon atmosphere passing through a column of phosphorus pentoxide and then through a vacuum/argon line by means of standard Schlenk techniques. The cleaned glassware is stored in an oven at 95 °C overnight before being connected to the vacuum/argon line, assembled and pumped under vacuum for 30 min and then filled with argon. All chemical products are handled in an argon-filled glove box (Jacomex, Campus-type; O_2 and H_2O concentrations kept at ≤0.1 ppm and ≤0.8 ppm, respectively). Toluene (99.85%, Extra Dry over Molecular Sieve, AcroSeal(R)) was purchased from Acros Organics™. The polycarbosilane (labeled StarPCS^{TM} SMP-730, Starfire Systems® Incorporation, Glenville, NY, USA), with a density of 1.0 g·cm^{-3} was stored in a freezer and used as-received. Anal. Found (wt%): Si 32.1, C 55.2, H 7.7, N 1.0, O 4.0. $[Si_{1.0}C_{4.1}H_{7.0}N_{0.1}O_{0.2}]_n$ (*Normalyzed to total 100 wt % (total of wt% was 98.5 wt%) and reference to* $Si_{1.0}$ *Nitrogen content (below 2 wt%) omitted in the empirical formulae*). FTIR (ATR/cm^{-1}): ν (C−H) = 3070 (w), 3050 (w), 2950 (m), 2915 (s), 2850 (s); ν (Si−H) = 2120 (vs); δ (C-H in Si-phenyl) = 1430 (s), δ (C-H in Si-CH_2) = 1360 (m); δ (−CH_3 in Si−CH_3) = 1251 (m); δ (Si-CH_2-Si) = 1049 cm^{-1} (s); δ (Si-H) = 941 cm^{-1} (s); δ (Si-C, rocking) = 854 cm^{-1}(s); δ (Si−CH_3, rocking) = 770 (s), $\omega_{\delta,\gamma}$ (C-H in R-Si(methyl)(phenyl)-R (R = C or O)) = 730, Φ (C-H in R-Si(phenyl)$_2$-R (R = C or O)) = 695 (vs).

Fillers as SiC Boostec® and Si particles were obtained from Mersen (Courbevoie, France) and Höganäs (Höganäs, Sweden), respectively. Their number and volume distribution has been measured (*See Figure 9SI in ESI*).

Ink preparation: The mixture made of **SMP-730**, Si and SiC powders is prepared in toluene in a three-neck round-bottom flask under argon. In a typical experiment,10.0 g of **SMP-730** are dissolved in extra dry toluene (30 ml) at room temperature (RT) under vigorous stirring. Then 2.5 g of Si particles and 20.0 g of SiC particles are added in flowing argon at RT to be stirred for 30 minutes. Then, the mixture underwent an ultrasonic treatment for 15 minutes to optimize fillers dispersion. Finally, the solvent is removed under vacuum *via* an ether bridge (60 °C/1.5·10^{-1} mbar) to release a viscous sample labeled **$Si_{12.6}SiC_{40.0}$@SMP-730** at RT which was further thermolyzed at 120 °C for 4 hours under vigorous stirring in flowing argon. After cooling down, a highly viscous sample labeled **$Si_{12.6}SiC_{40.0}$@R120** is delivered.

Ink printing: A lab-scale designed granule-based FDM device (ID Conception, Saint-Marien, France) was designed to showcase the potential of the as-prepared **$Si_{12.6}SiC_{40.0}$@R120** sample to form on-demand 3D parts (*See Figure 1*). It consists of an home made extrusion head mounted on a computer numerical control (CNC) device to build 3D parts in a layer- by-layer procedure. The mechanical principal of the extrusion head is based on a screw that moves a piston inside a barrel to control the volume of the extruded material. A script in python language has been developped and used as a slicer in order to compute the filament deposition paths from a CAD model and to generate it in G-code language. Compared to conventional slicers, this method allows an adapted control of both the printing parameters and the deposition path geometry for the granule-based FDM of ink derived from preceramic polymers. The as-prepared **$Si_{12.6}SiC_{40.0}$@R120** sample (10.0 g) is loaded as a feedstock compound into a 10 mm inner diameter barrel which is then heated at 90 °C. After 10 min at this temperature, the **$Si_{12.6}SiC_{40.0}$@R120** sample is driven along the barrel to be extruded through a nozzle with an internal diameter of 400 μm. Printing speed was set at 14.4 $mm.s^{-1}$ corresponding to a shear rate of 144 s^{-1}. The 3D parts are collected on an alumina plate to be directly transferred into the furnace for the further heat-treatment.

Ceramic conversion: As printed 3D parts and the alumina plate are directly introduced in flowing argon into an alumina tube from a horizontal furnace (Carbolite GHA12/450). The tube is then evacuated (0.1 mbar) for 30 min and refilled with argon (99.995 %) to atmospheric pressure. Subsequently, the samples are subjected to a cycle of ramping of 0.5 $°C.min^{-1}$ to 1000 °C in flowing argon (dwelling time of 2 h at 1000 °C). A constant flow (120 $mL.min^{-1}$) of argon is passed through the tube during the pyrolysis cycle. Cooling occurred at 0.5 $°C.min^{-1}$ under argon atmosphere to deliver 3D-printed **$Si_{12.6}SiC_{40.0}$@R120_10** samples. The latter are subsequently introduced in a graphite furnace (Nabertherm VHT-GR) for achieving heat-treatments above 1000 °C. The furnace is pumped under vacuum (1.10^{-1} mbar), refilled with argon and maintained under a constant flow of argon (200 $mL.min^{-1}$) during the whole heat treatment. The program consists of a 5 $°C.min^{-1}$ heating ramp up to the maximum temperature fixed at 1400 °C or 1800 °C (for XRD investigation), dwelling at the selected temperature for 2 h and cooling down to RT at 5 $°C.min^{-1}$. As-obtained 3D-printed samples are labeled **$Si_{12.6}SiC_{40.0}$@R120_T** with T being the two first digits of the temperature at which the material has been exposed (10 for 1000, 14 for 1400 and 18 for 1800 °C). The **R120** sample underwent the same heat-treatment to serve as reference. As-obtained samples were labeled **R120_T** with T being the two first digits of the temperature at which the material has been exposed (10 for 1000, 14 for 1400 and 18 for 1800 °C).

Characterization: The functional groups and main units in the **SMP-730** sample were determined by attenuated total reflectance (ATR) spectroscopy using a Nicolet iS10 Fourier transform-infrared spectrometer. Differential scanning calorimetry measurement (DSC) were performed at LMI (University of Lyon, France). They have been performed on a Mettler Toledo DSC1 under nitrogen atmosphere between -50 and 200 °C with a ramp of 10 °C.min^{-1}. The silicon (Si) content of polymers and derived ceramics has been performed at Mikroanalytisches Labor Pascher (Remagen, Germany). Elemental analyses of **SMP-730** and **R120** samples and the derived ceramic samples were extended via instrumental gas analysis (IGA) techniques to carbon (C) content measurements using a Horiba Emia-321V and to oxygen (O), nitrogen (N) and hydrogen (H) content measurements using a Horiba EMGA-830. All the compositions have been normalized to $Si_{1.0}$. Thermogravimetric analyses (TGA) of **SMP-730** and **R120** samples were performed in flowing argon at 5 °C.min^{-1} to 1000 °C using alumina crucibles at ambient atmospheric pressure (STA 449 F3, Netzsch GmbH, Selb, Germany). High-temperature TG analyses of samples pyrolyzed at 1000 °C were done up to 1400 °C using tungsten crucibles at ambient atmospheric pressure (Setaram, Setsys apparatus) at a heating rate of 5 °C.min^{-1} in flowing argon. Rheological measurements were carried out with a HAAKE MARS III from Thermo Fisher Scientific with plate-plate geometry (nominal gap: 1.0 mm, diameter: 20 mm) under argon. The phase composition of crushed 3D-printed samples and ceramic powders derived from polymers was analyzed from XRD data obtained with a Bruker D8 Advance diffractometer. The scan was performed using the CuKα1/2 radiations, from 20 to 90° 2θ with a step size of 0.02° and acquisition time of 0.9 s per step. The diffraction patterns were analyzed using the Diffrac + EVA software with the JCPDS-ICDD database. Raman mapping of crushed 3D-printed samples and ceramic powders derived from polymers was performed using an inVia Reflex Renishaw Raman spectrophotometer (Wotton-under-Edge, UK). The 2D mapping module was used in streamline mode with a 40 × 2 μm^2 laser beam. The high number of spectra recorded (24 000 spectra for a 200 × 200 μm^2 2D map with a step size of 1.3 μm) enables high spatial resolution images to be generated. Spectra were recorded at the wavelength of 532 nm at 10 % of power to avoid any damage of the samples using a x100 long working distances objective. An exposure time of 2 s has been selected to proceed of a 200 μm square mapping. Spectra were recorded between 480 and 1680 cm^{-1} to focus on the D (disordered graphite lattice vibrations with A_{1g} symmetry) and G (graphite-type lattice vibrations with E_{2g} symmetry) modes of sp^2 carbon, on the first-order longitudinal optical (LO) phonon mode of silicon and on the transverse optical (TO) phonon mode of silicon carbide. Raw data were analyzed using the WiRE

software from Renishaw. The 3D-printed **$Si_{12.6}SiC_{40.0}$@R120_14** sample surface was observed by JEOL IT300 scanning electron microscope. The bulk and apparent density values as well as open porosity of the 3D-printed **$Si_{12.6}SiC_{40.0}$@R120_14** sample were determined using the Archimedes method in ethanol. Filler sizes have been measured with a Horiba Partica LA-950V2 apparatus. Mechanical test have been performed on the 3D-printed **$Si_{12.6}SiC_{40.0}$@R120_14** sample as bars (*See Figures 6SI in ESI*) with a four-point bending test system (Instron 5969), piloted by Bluehill 3 software, and following the standard procedure ASTM C1161-18.[60] The specimens were placed in a four-point loading fixture and loaded to fracture. The size of the specimens (cross-sections are rectangular) was 4.5 mm in thickness, 6.6 mm in width and 70 mm in length. The spans are 20 mm x 40 mm.

Supporting Information

Supporting Information is available from the Wiley Online Library or from the author.

Acknowledgements

The authors thank the Nouvelle-Aquitaine region and CTTC for the financial support of the PhD thesis of Dr. Maxime Cheype and Dr. Thierry Chartier for his continuous support and expertise in additive manufacturing. This work was partially supported by the ANR (Grant project Number ANR-19-ASTR-0007). M. Colas (Raman spectroscopy), J. Cornette (Raman spectroscopy), R. Chiriac (DSC), R. Lucas (rheological measurements), and P. Michaud (four-point bending tests) are also acknowledged for the further characterization of materials.

Conflict of Interest

Authors declare no conflicts of interest

Received: ((will be filled in by the editorial staff))

Revised: ((will be filled in by the editorial staff))

Published online: ((will be filled in by the editorial staff))

References

[1] M. Bougoin, F. Mallet, J. Lavenac, A. Gerbert Gaillard, D. Ballhause, F. Chaumeil, in *Int. Conf. Space Opt. — ICSO 2018* (Eds.: N. Karafolas, Z. Sodnik, B. Cugny), SPIE, Chania, Greece, **2019**, p. 60.

[2] D. Castel, E. Sein, S. Lopez, T. Nakagawa, M. Bougoin, in (Eds.: R. Navarro, C. R. Cunningham, E. Prieto), Amsterdam, Netherlands, **2012**, p. 84502P.

[3] M. Balestrat, M. Cheype, C. Gervais, X. Deschanels, S. Bernard, *Mater. Adv.* **2023**, *4*, 1161.
[4] M. Balestrat, M. Cheype, P. Carles, X. Deschanels, A. Soum-Glaude, C. Gervais, F. Rossignol, N. Pradeilles, S. Bernard, *Open Ceram.* **2023**, *14*, 100353.
[5] S. Mahmoudinezhad, M. Sadi, H. Ghiasirad, A. Arabkoohsar, *Renew. Sustain. Energy Rev.* **2023**, *183*, 113467.
[6] C. Lewinsohn, *Compact Ceramic Microchannel Heat Exchangers*, Ceramatec Inc, West Valley City, UT, (USA), **2016**.
[7] J. Thomas, M. Banda, W. Du, W. Yu, A. Chuang, D. M. France, D. Singh, *Ceram. Int.* **2022**, *48*, 22975.
[8] A. Montón, F. Maury, G. Chevallier, C. Estournès, M. Ferrato, D. Grossin, *J. Eur. Ceram. Soc.* **2021**, *41*, 7543.
[9] M. Balestrat, E. Diz Acosta, O. Hanzel, N. Tessier-Doyen, R. Machado, P. Šajgalík, Z. Lenčéš, S. Bernard, *J. Eur. Ceram. Soc.* **2020**, *40*, 2604.
[10] B. Román-Manso, R. D. Weeks, R. L. Truby, J. A. Lew, *Adv. Mater.* **2023**, *35*, 2209270.
[11] H. Chen, L. Guo, W. Zhu, C. Li, *Polymers* **2022**, *14*, 4635.
[12] M. A. S. R. Saadi, A. Maguire, N. T. Pottackal, Md S. H. Thakur, M. Md. Ikram, A. J. Hart, P. M. Ajayan, M. M. Rahman, *Adv. Mater.* **2022**, *34*, 2108855.
[13] R. He, N. Zhou, K. Zhang, X. Zhang, L. Zhang, W. Wang, D. Fang, *J. Adv. Ceram.* **2021**, *10*, 637.
[14] C. L. Cramer, E. Ionescu, M. Graczyk-Zajac, A. T. Nelson, Y. Katoh, J. J. Haslam, L. Wondraczek, T. G. Aguirre, S. LeBlanc, H. Wang, M. Masoudi, E. Tegeler, R. Riedel, P. Colombo, M. Minary-Jolandan, *J. Eur. Ceram. Soc.* **2022**, *42*, 13049.
[15] Y. De Hazan, D. Penner, *J. Eur. Ceram. Soc.* **2017**, *37*, 5205.
[16] X. Bai, G. Ding, K. Zhang, W. Wang, N. Zhou, D. Fang, R. He, *Open Ceram.* **2021**, *5*, 100046.
[17] A. Gómez-Gómez, J. J. Moyano, B. Román-Manso, M. Belmonte, P. Miranzo, M. I. Osendi, *J. Eur. Ceram. Soc.* **2019**, *39*, 688.
[18] Q. Zhu, X. Dong, J. Hu, J. Yang, X. Zhang, Y. Ding, S. Dong, *Ceram. Int.* **2020**, *46*, 6978.
[19] T. Tu, G. Jiang, *Ceram. Int.* **2018**, *44*, 3400.
[20] K. Liu, D. L. Bourell, Y. Tan, J. Wang, M. He, H. Sun, Y. Shi, J. Chen, *Ceram. Int.* **2018**, *44*, 21067.
[21] J.-W. Oh, J. Park, S. Nahm, H. Choi, *Int. J. Refract. Met. Hard Mater.*. **2021**, *101*, 105686.
[22] T. Koyanagi, K. Terrani, S. Harrison, J. Liu, Y. Kutoh, *J. Nucl. Mater.* **2021**, *543*, 152577.
[23] S. Lamnini, H. Elsayed, Y. Lakhdar, F. Baino, F. Smeacetto, E. Bernardo, *Heliyon* **2022**, *8*, e10651.
[24] Y. Lakhdar, C. Tuck, J. Binner, A. Terry, R. Goodridge, *Prog. Mater. Sci.* **2021**, *116*, 100736.
[25] F. Clemens, F. Sarraf, A. Borzi, A. Neels, A. Hadian, *J. Eur. Ceram. Soc.* **2023**, *43*, 2752.
[26] M. Pelanconi, P. Colombo, A. Ortona, *J. Eur. Ceram. Soc.* **2021**, *41*, 5056.
[27] M. Pelanconi, G. Bianchi, P. Colombo, A. Ortona, *J. Am. Ceram. Soc.* **2022**, *105*, 786.
[28] L. Wahl, M. Lorenz, J. Biggemann, N. Travitzky, *J. Eur. Ceram. Soc.* **2019**, *39*, 4520.
[29] W. Du, B. Ma, J. Thomas, D. Singh, *J. Eur. Ceram. Soc.* **2023**, *43*, 2345.
[30] J. Roger, G. Chollon, *Ceram. Int.* **2019**, *45*, 8690.
[31] F. Wang, F. Luo, Y. Huang, X. Cao, C. Yuan, *Adv. Mater. Technol.* **2023**, *8*, 2201383.
[32] R. P. Chaudhary, C. Parameswaran, M. Idrees, A. S. Rasaki, C. Liu, Z. Chen, P. Colombo, *Progress Mater. Sci.* **2022**, *128*, 100969.

[33] B. J. Ackley, K. L. Martin, T. S. Key, C. M. Clarkson, J. J. Bowen, N. D. Posey, J. F. Ponder Jr., Z. D. Apostolov, M. K. Cinibulk, T. L. Pruyn, M. B. Dickerson, *Chem. Rev.* **2023**, *123*, 4188.
[34] J. J. Bowen, S. Mooraj, J. A. Goodman, S. Peng, D. P. Street, B. Roman-Manso, E. C. Davidson, K. L. Martin, L. M. Rueschhoff, S. N. Schiffres, W. Chen, J. A. Lewis, M. B. Dickerson, *Mater. Today* **2023**, *58*, 100969.
[35] E. Zanchetta, M. Cattealdo, G. Franchin; M. Schwentenwein, J. Homa, G. Brusatin, P. Colombo, *Adv. Mater.* **2016**, *28*, 370.
[36] Z. C. Eckel, C. Zhou, J. H. Martin, A. J. Jacobsen, W. B. Carter, T. A. Schaedler, *Science* **2016**, *351*, 6268.
[37] S. Bernard, F. Chassagneux, M.-P. Berthet, D. Cornu, P. Miele, , *J. Am. Ceram. Soc.* **2005**, *88*, 1607.
[38] S. Duperrier, C. Gervais, S. Bernard, D. Cornu, F. Babonneau, C. Balan, P. Miele, *Macromolecule*, **2007**, *40*, 1018.
[39] L. Gottardo, S. Bernard, C. Gervais, K. Inzenhofer, G. Motz, M. Weinmann, C. Balan, P. Miele, *J. Mater. Chem.* **2012**, *22*, 7739.
[40] A. Viard, P. Miele, S. Bernard, *J. Ceram. Soc. Jp.* **2016**, *124*, 967.
[41] F. Sarraf, A. Hadian, S. V. Churakov, F. Clemens, *J. Eur. Ceram. Soc.* **2023**, *43*, 530.
[42] L. Gorjan, R. Tonello, T. Sebastian, P. Colombo, F. Clemens, *J. Eur. Ceram. Soc.* **2019**, *39*, 2463.
[43] L. Zhao, X. Wang, H. Xiong, K. Zhou, D. Zhang, *J. Eur. Ceram. Soc.* **2021**, *41*, 5066.
[44] https://www.starfiresystems.com/wp-content/uploads/2018/03/SMP-730.pdf
[45] P. Greil, *J. Am. Ceram. Soc.* **1995**, *78*, 835.
[46] S. Duperrier, S. Bernard, A. Calin, C. Sigala, R. Chiriac, P. Miele, C. Balan, *Macromolecules* **2007**, *40*, 1028.
[47] V. V. Pujar, J. D. Cawley, *J. Am. Ceram. Soc.* **1995**, *78*, 774.
[48] Q. Wen, Z. Yu, R. Riedel, *Progress Mater. Sci.* **2020**, *109*, 100623.
[49] J. Bialoskorski, M. Pyzalski, E. Walasek, *J. Therm. Anal.* **1990**, *36*, 2033.
[50] M. Biesuz, P. Bettotti, S. Signorini, M. Bortolotti, R. Campostrini, M. Bahri, O. Ersen, G. Speranza, A. Lale, S. Bernard, G. D. Soraru, *Nanotechnology* **2019**, *30*, 255601.
[51] M. Wieligor, Y. Wang, T. W. Zerda, *J. Phys. Condens. Matter* **2005**, *17*, 2387.
[52] W. Freudenberg, F. Wich, N. Langhof, S. Schafföner, *J. Eur. Ceram. Soc.* **2022**, *42*, 1822.
[53] H. Xiong, L. Zhao, H. Chen, X. Wang, K. Zhou, D. Zhang, *J. Alloys Compd.* **2019**, *809*, 151824.
[54] R. W. Rice, *Porosity of Ceramics: Properties and Applications.* 1st ed. CRC Press; Boca Raton, FL, USA: 1998.
[55] K. K. Phani, S. K. Niyogi, *J. Mater. Sci.* **1987**, *22*, 257.
[56] A. S. Wagh, J. P. Singh, R. B. Poeppel, *J. Mater. Sci.* **1993**, *28*, 3589.
[57] A. S. Wagh, R. B. Poeppel, J. P. Singh, *J. Mater. Sci.* **1991**, *26*, 3862.
[58] D. Godec, S. Cano, C. Holzer, J. Gonzalez-Gutierrez, *Materials* **2020**, *13*, 774.
[59] A. E. Costa, A. Ferreira da Silva, O. Sousa Carneiro, *Rapid Prototyp. J.* **2019**, *25*, 555.
[60] G. D. Quinn, R. Morrell, *J. Am. Ceram. Soc.* **1991**, *74*, 2037.

Table of contents entry.

A straightforward design strategy coupling a granule-based FDM process and preceramic polymer manipulation highlights the production of 3D near-net-shape stoichiometric SiC parts with a high potential impact in adverse environments as mirrors for lightweight opto-

mechanical systems, as high-flux concentrated solar receivers and as heat exchangers for thermal management .

ToC figure ((Please choose one size: 55 mm broad × 50 mm high or 110 mm broad × 20 mm high. Please do not use any other dimensions))

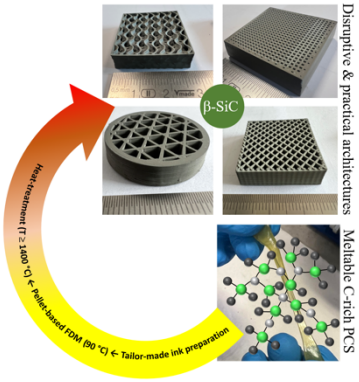

Supporting Information

Straightforward design strategy towards 3D near-net-shape stoichiometric SiC parts

Maxime Cheype, Vincent Pateloup, Samuel Bernard**

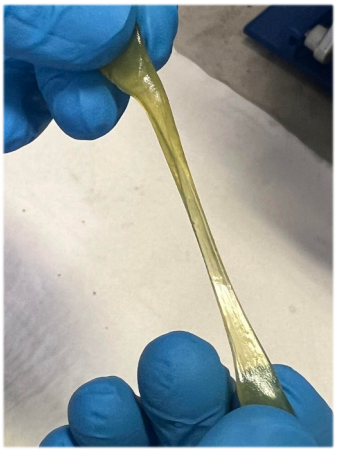

(a)

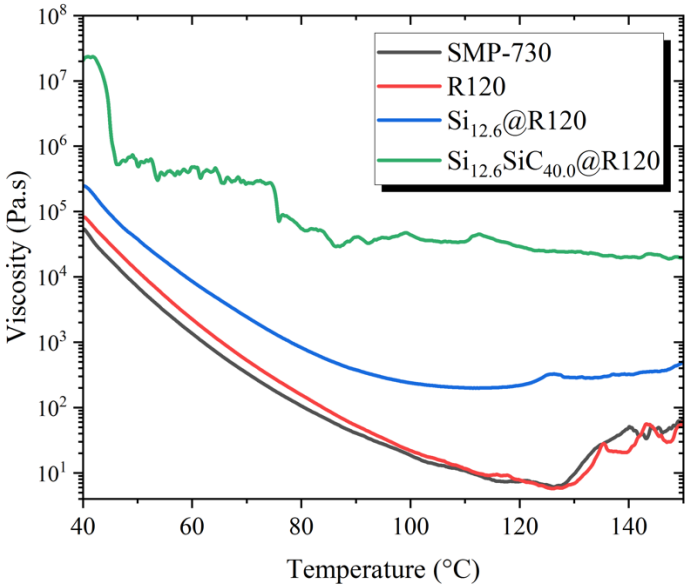

(b)

Fig. 1SI. Capacity of **SMP-730** to be stretched upon melting, (a) and evolution of the viscosity of the polymers (**SMP-730**, **R120**) and filled polymers (**$Si_{12.6}$@R120**, **$Si_{12.6}SiC_{40.0}$@R120**) as a function of the applied temperature (b).

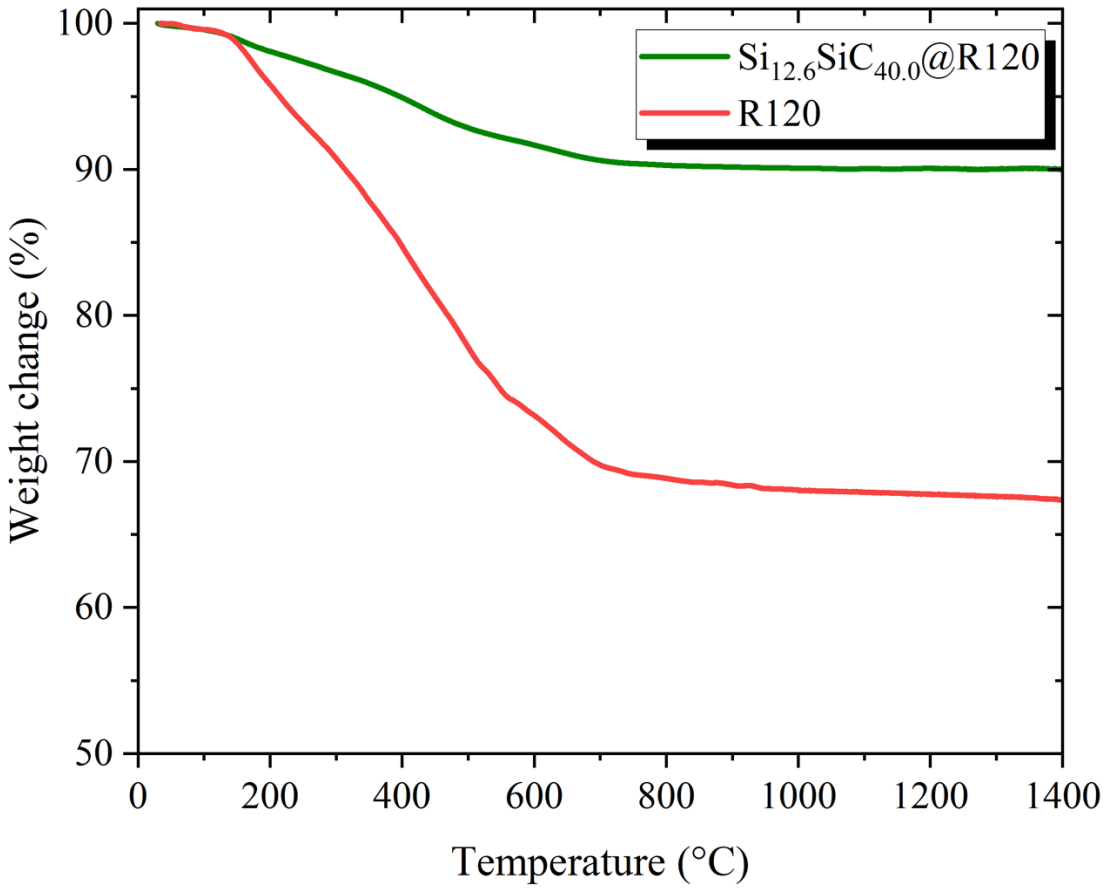

Fig. 2SI. TG investigation of the **$Si_{12.6}SiC_{40.0}$@R120** sample (compared to the **R120** sample) during heat-treatment to 1400°C in flowing argon.

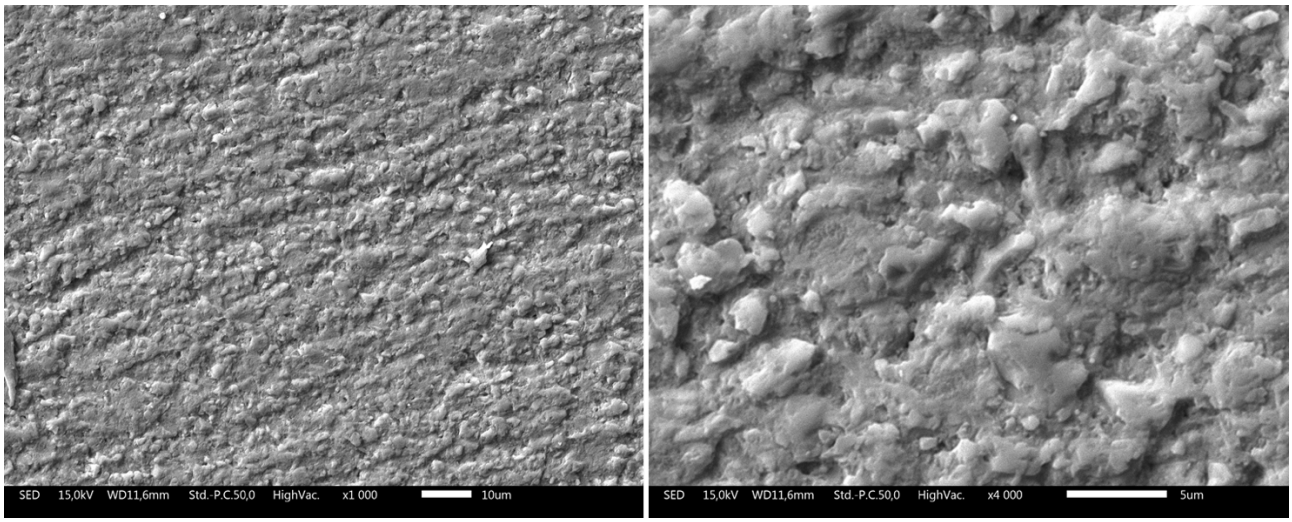

Fig. 3SI. High magnification SEM image of the surface of the 3D-printed **$Si_{12.6}SiC_{40.0}$@R120_14** sample.

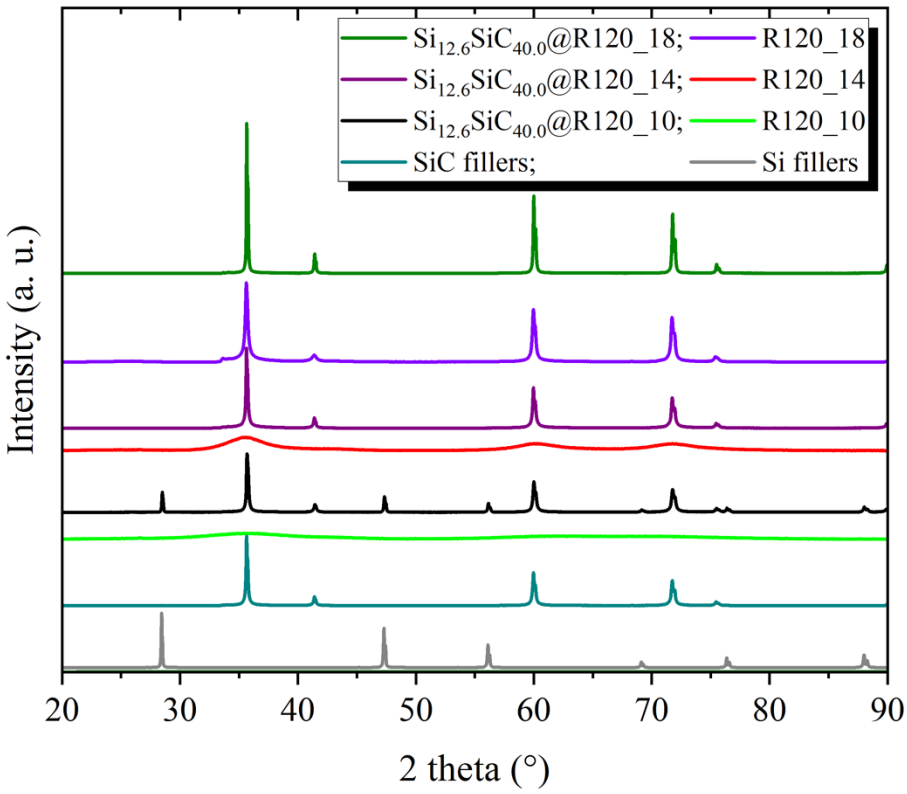

Fig. 4SI. XRD pattern evolution of **$Si_{12.6}SiC_{40.0}$@R120-10** sample at 1400 °C (**$Si_{12.6}SiC_{40.0}$@R120-14**) and 1800 °C (**$Si_{12.6}SiC_{40.0}$@R120-18**) associated with the XRD patterns of the **R120_10**; **R120_14** and **R120_18** samples and of the Si and SiC fillers.

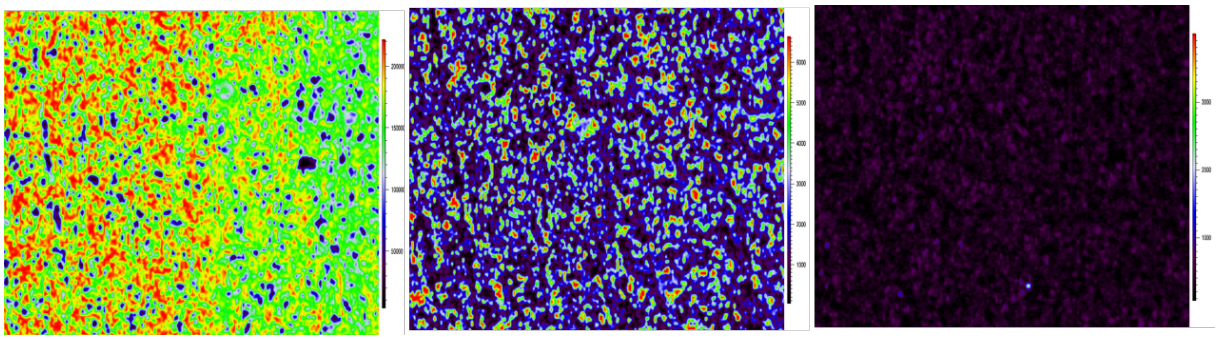

Fig. 5SI. 200 × 200 µm^2 Raman maps of **$Si_{12.6}SiC_{40.0}$@R120_10** collected with a with a step size of 1.3 µm : C (left), Si (middle), SiC (right) (c).

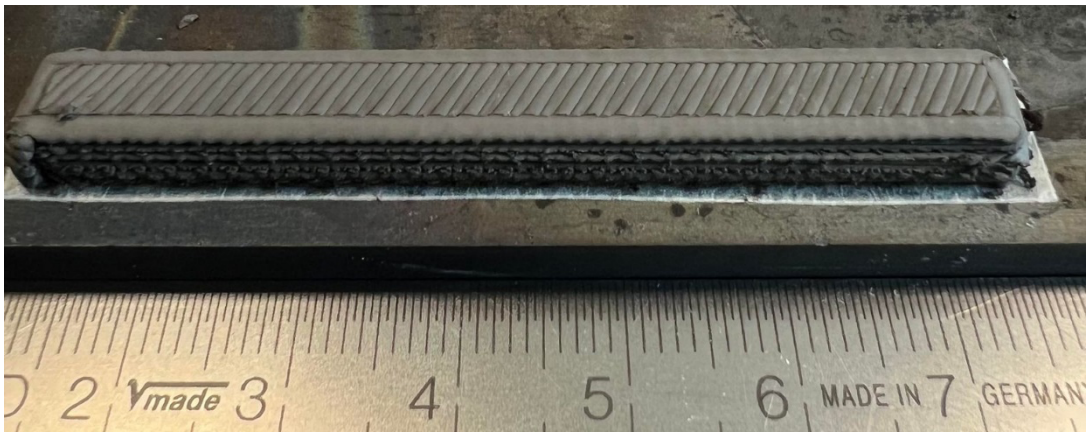

Fig. 6SI. Representative 3D printed **$Si_{12.6}SiC_{40.0}$@R120-14** sample for flexural tests.

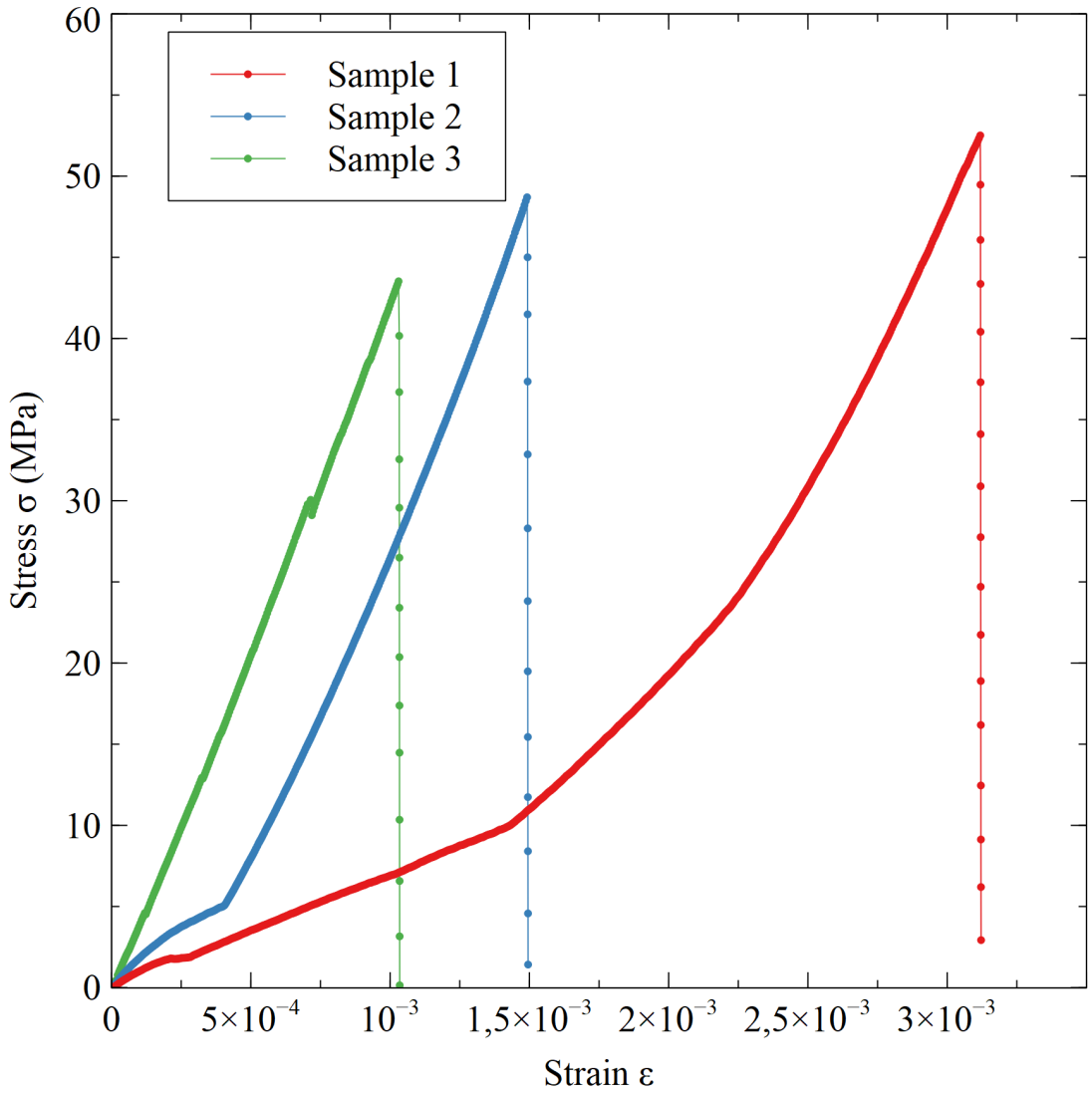

Fig. 7SI. Representative flexural stress-strain curves of 3D-printed **$Si_{12.6}SiC_{40.0}$@R120_14** samples.

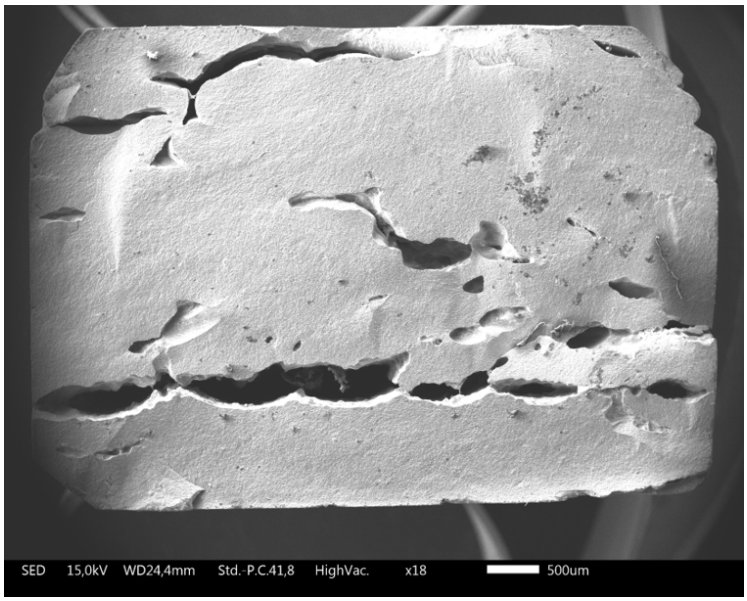

Fig. 8SI. Fracture surface of the sample 3 with the lowest flexural strength (*See Figure 7SI in ESI*).

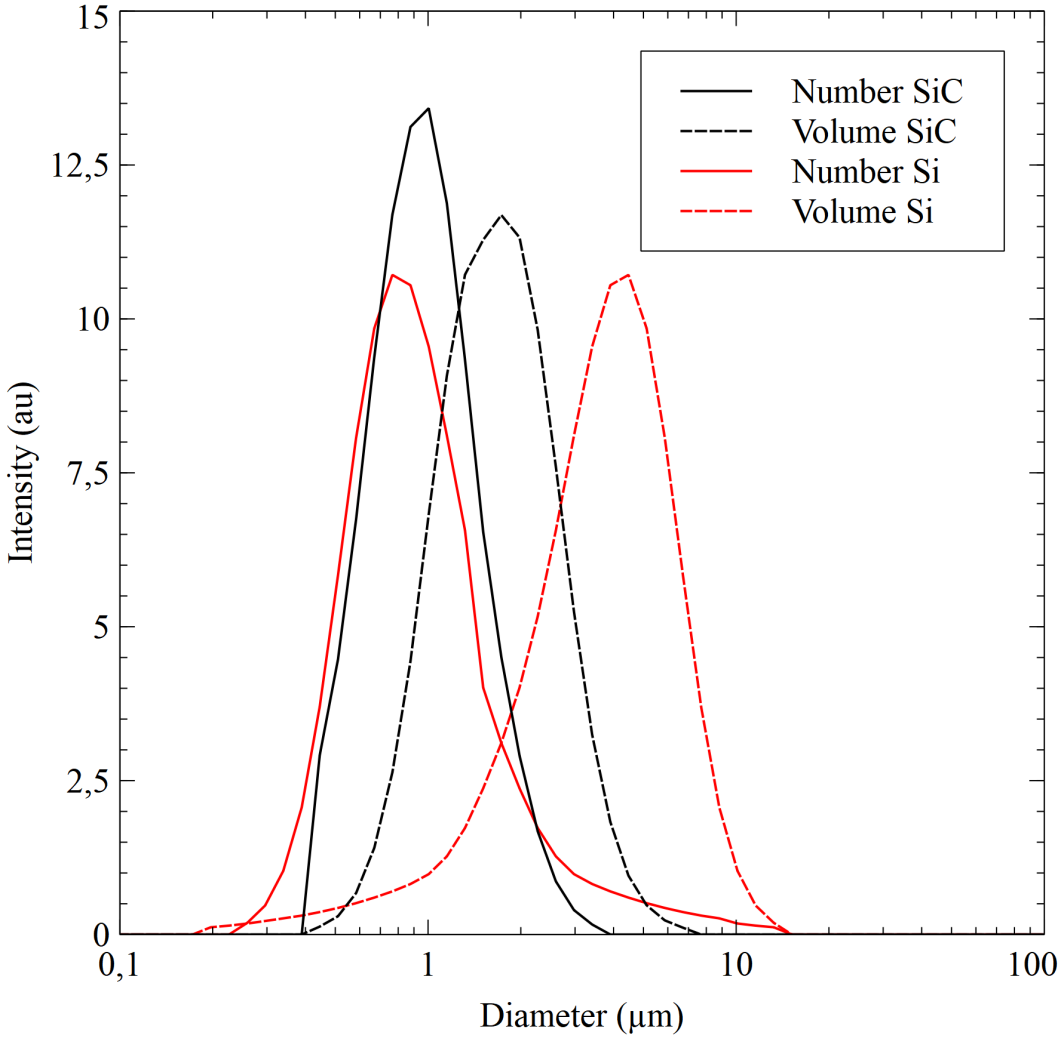

Fig. 9SI. Number and volume distribution of SiC and Si fillers.